The Astrophysical Journal, 746:152 (8pp), 2012 February 20 doi:10.1088/0004-637X/746/2/152

FLARE-GENERATED TYPE II BURST WITHOUT ASSOCIATED CORONAL MASS EJECTION

J. Magdalenić[1,2], C. Marqué[1], A. N. Zhukov[1,3], B. Vršnak[2], and A. Veronig[4]
[1] Solar-Terrestrial Center of Excellence, SIDC, Royal Observatory of Belgium, Avenue Circulaire 3, B-1180 Brussels, Belgium; Jasmina.Magdalenic@oma.be
[2] Hvar Observatory, Faculty of Geodesy, Kačićeva 26, HR-10000 Zagreb, Croatia
[3] Skobeltsyn Institute of Nuclear Physics, Moscow State University, 119992 Moscow, Russia
[4] IGAM/Kanzelhöhe Observatory, Institut of Physics, Universität Graz, Universitätsplatz 5, A-8010 Graz, Austria
Received 2011 October 3; accepted 2011 November 23; published 2012 February 2

ABSTRACT

We present a study of the solar coronal shock wave on 2005 November 14 associated with the *GOES* M3.9 flare that occurred close to the east limb (S06° E60°). The shock signature, a type II radio burst, had an unusually high starting frequency of about 800 MHz, indicating that the shock was formed at a rather low height. The position of the radio source, the direction of the shock wave propagation, and the coronal electron density were estimated using Nançay Radioheliograph observations and the dynamic spectrum of the Green Bank Solar Radio Burst Spectrometer. The soft X-ray, Hα, and *Reuven Ramaty High Energy Solar Spectroscopic Imager* observations show that the flare was compact, very impulsive, and of a rather high density and temperature, indicating a strong and impulsive increase of pressure in a small flare loop. The close association of the shock wave initiation with the impulsive energy release suggests that the impulsive increase of the pressure in the flare was the source of the shock wave. This is supported by the fact that, contrary to the majority of events studied previously, no coronal mass ejection was detected in association with the shock wave, although the corresponding flare occurred close to the limb.

Key words: shock waves – Sun: corona – Sun: coronal mass ejections (CMEs) – Sun: flares – Sun: radio radiation

Online-only material: color figures

1. INTRODUCTION

Shock wave propagation through the solar corona can result in different signatures: type II radio bursts (e.g., Wild 1950; Nelson & Melrose 1985; Vršnak & Cliver 2008; Nindos et al. 2008), Moreton waves (e.g., Moreton & Ramsey 1960; Warmuth et al. 2004; Warmuth 2007), EUV waves (e.g., Vršnak et al. 2002b; Ma et al. 2011), or white light and soft X-ray (SXR) shock signatures (e.g., Vourlidas et al. 2003; Ontiveros & Vourlidas 2009; Khan & Aurass 2002; Warmuth et al. 2005). The longest-known and most studied signatures of shock waves are type II radio bursts. They appear in dynamic radio spectra as lanes of enhanced radio emission slowly drifting (drift rate $df/dt < 1$ MHz s^{-1}) from high to low frequencies. Meter wavelength type II bursts are caused by shocks propagating through the solar corona, appearing typically at about 100 MHz.

Type II bursts are usually observed in association with flares and coronal mass ejections (CMEs). Due to the close synchronization of the acceleration phase of the CME, the flare impulsive phase, and appearance of the shock signatures (Zhang et al. 2001; Maričić et al. 2007; Temmer et al. 2008, 2010), it is rather difficult to identify the origin of coronal shock waves. Numerous studies of CME/flare events have been presented over the last 60 years, favoring interpretations in terms of either CME-driven (e.g., Gopalswamy et al. 1998; Mancuso et al. 2002; Cliver et al. 2004; Liu et al. 2009) or flare-ignited shocks (e.g., White et al. 2007; Magdalenić et al. 2008, 2010; Vršnak & Cliver 2008; Nindos et al. 2011), or some combination of these two mechanisms. Recently, the hypothesis that all coronal shocks are CME-driven (Cliver et al. 2004) was tested by Magdalenić et al. (2008, 2010), who showed that a specific class of CME/flare events associated with flare-generated shocks exists. Flare-ignited shock waves of this class were associated with rather slow CMEs, with mean velocity below 500 km s^{-1}.

It is clear that CMEs play a very important role in the formation of coronal waves (e.g., Thompson et al. 2000; Gopalswamy et al. 2005). The still open question is whether the presence of a CME is a necessary condition for shock formation.

In this study, we present a specific high-frequency type II burst recorded on 2005 November 14.[5] The shock signatures were associated with the impulsive flare, but without a clear association with a CME. The radio signatures of the shock wave are described in Sections 2.1 and 2.2. Section 2.3 presents a detailed description of the associated flare and the coronagraphic observations. Discussion and conclusions are presented in Section 3.

2. OBSERVATIONS

The study of the 2005 November 14 event is based on the following observations:

1. For a general overview (Figure 1(a)), dynamic spectra recorded by: (1) the Phoenix 2 broadband radio spectrometer in the frequency range 4000–400 MHz (Messmer et al. 1999), (2) the spectrographs of the Astrophysical Institute Potsdam (AIP) in the frequency range 400–70 MHz (Mann et al. 1992), (3) the Nançay Decameter Array (DAM) in the frequency range 70–10 MHz (Lecacheux 2000), and (4) WIND Waves observations in the frequency range 14–1 MHz (Bougeret et al. 1995).
2. For a detailed study (Figure 1(b)), dynamic spectra recorded by the Green Bank Solar Radio Burst Spectrometer (GBSRBS; White et al. 2005) in the frequency range 1000–18 MHz.
3. Observations by the Nançay Radioheliograph (NRH; Kerdraon & Delouis 1997) at 432, 411, 327, 237, 164, and 151 MHz with a time resolution of 0.5 s.
4. SXR flux measurements made by *GOES*.

[5] A short preliminary report about this event was presented by White et al. (2007) in the NRAO Newsletter.

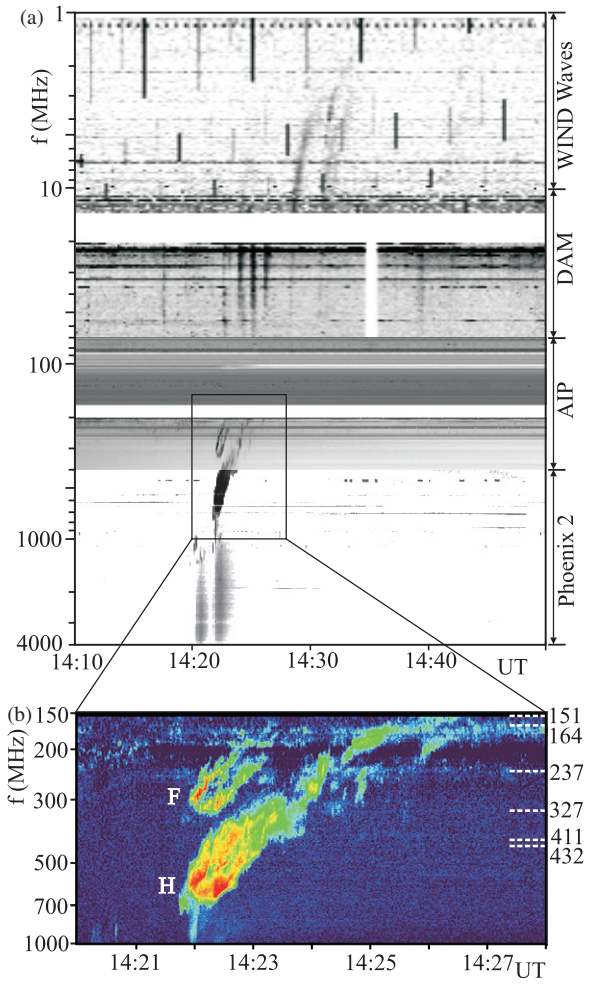

Figure 1. (a) The composite dynamic spectrum giving an overview of the radio emission in the 2005 November 14 event. The frequency range 4000–1 MHz is covered by the dynamic spectra recorded by Phoenix 2 (4000–400 MHz), the AIP spectrographs (400–70 MHz), DAM (70–10 MHz), and WIND Waves (10–1 MHz). (b) The detailed dynamic spectrum recorded by the GBSRBS showing well-defined fundamental and harmonic bands of the type II burst. The Nançay observing frequencies (in MHz) are marked on the right vertical axis.

(A color version of this figure is available in the online journal.)

5. SXR observations by the Solar X-Ray Imager (SXI; Hill et al. 2005; Pizzo et al. 2005) on board the *GOES-12* satellite.
6. Full-disk imaging in Hα by the Kanzelhöhe Observatory (KSO; Otruba & Pötzi 2003).
7. Hard X-ray observations by the *Reuven Ramaty High Energy Solar Spectroscopic Imager* (*RHESSI*; Lin et al. 2002) of the high-energy solar flare emission (3 keV–17 MeV) with high spectral and spatial resolution.
8. EUV observations of low coronal dynamics and possible early CME signatures provided by the Extreme-Ultraviolet Imaging Telescope (EIT; Delaboudinière et al. 1995) on board the *Solar and Heliospheric Observatory* (*SOHO*).
9. Coronagraphic observations of possibly associated CMEs in the upper corona obtained by the *SOHO* Large Angle and Spectroscopic Coronagraph (LASCO; Brueckner et al. 1995) C2 and C3 instruments.

2.1. Radio Emission

The radio bursts observed in the microwave range (4.0–1.0 GHz) indicating the impulsive phase of the flare consisted of two strong continuum enhancements. The bursts started at 14:20 UT and lasted for about 4 minutes (Figure 1(a)). The dynamic spectrum recorded by Phoenix 2 also shows patchy and bursty drifting emission in the frequency range 1.5–0.9 GHz between 14:19:40 and 14:22:30 UT. This fragmented radio emission might be the precursor (Karlicky 1984; Klassen et al. 1999, 2003) to the metric type II burst observed in the time interval 14:21:40–14:28:00 UT (Figure 1(a)). The WIND Waves observations do not show the continuation of the type II emission into the interplanetary space (14000–20 kHz). Rather weak type III bursts were observed in the frequency range 70–1 MHz in the interval 14:20–14:45 UT (Figure 1(a)).

We focus on the signatures of the shock wave, the metric type II radio burst. Figure 1(b) shows a strong and well-defined type II burst recorded by the GBSRBS. The harmonic band of the type II burst starts at an unusually high frequency of about 800 MHz and slowly drifts to about 130 MHz. Type II bursts with such a high starting frequency are rarely observed, and they usually exhibit highly fragmented emission patterns (Pohjolainen et al. 2008). The type II burst on 2005 November 14 shows rather smooth and well-defined harmonic and fundamental emission bands, in particular at the high-frequency part of the burst (800–350 MHz). The low-frequency part of the type II burst (350–200 MHz) is more structured than the high-frequency part. The AIP dynamic spectrum shows fine-scale structures and short-lived features, i.e., herringbone fine structures of the type II burst (Roberts 1959; Mann & Klassen 2005).

Both fundamental and harmonic bands of the type II burst are split into two parallel lanes of similar frequency drifts and intensity behavior (Figure 1(b)). This characteristic pattern, the so-called type II band split (Nelson & Melrose 1985; Vršnak et al. 2001), can be attributed to the simultaneous emission from the plasma ahead and behind the shock front, i.e., the upstream/downstream shock regions (Smerd et al. 1974, 1975; Vršnak et al. 2001). According to this hypothesis, the band split can be used to measure the shock amplitude and to estimate the Alfvén Mach number and the Alfvén speed (see, e.g., Vršnak et al. 2002a, 2004; Cho et al. 2007; Magdalenić et al. 2008, 2010). Using the measured relative band split (BDW ≈ 0.26) of the type II burst and considering plasma beta, $\beta = 0$, we find the Alfvén Mach number and Alfvén velocity to be about 1.4 and 700 km s^{-1}, respectively.

2.2. Estimation of the Coronal Electron Density and the Type II Burst Speed

The estimation of the radio-source height and its speed using only dynamic radio spectra strongly depends on the choice of a coronal electron density model (see, e.g., Magdalenić et al. 2008; Pohjolainen 2008). Therefore, the choice of the appropriate density model is of utmost importance when dealing with radio observations. In the case of an eruption that appears close to the solar limb, the influence of the plane-of-the-sky projection effects is minimized. This characteristic enables a scaling of the density model using the positions of associated radio sources (Pohjolainen et al. 2008; Magdalenić et al. 2008, 2010). For a detailed description of the procedure see Magdalenić et al. (2010).

The event of 2005 November 14 was associated with a flare in the NOAA AR 10822 that occurred rather close to the solar limb (S06° E60°). Therefore, we were able to apply the method of electron density scaling using the GBSRBS dynamic spectrum and NRH observations. The positions of

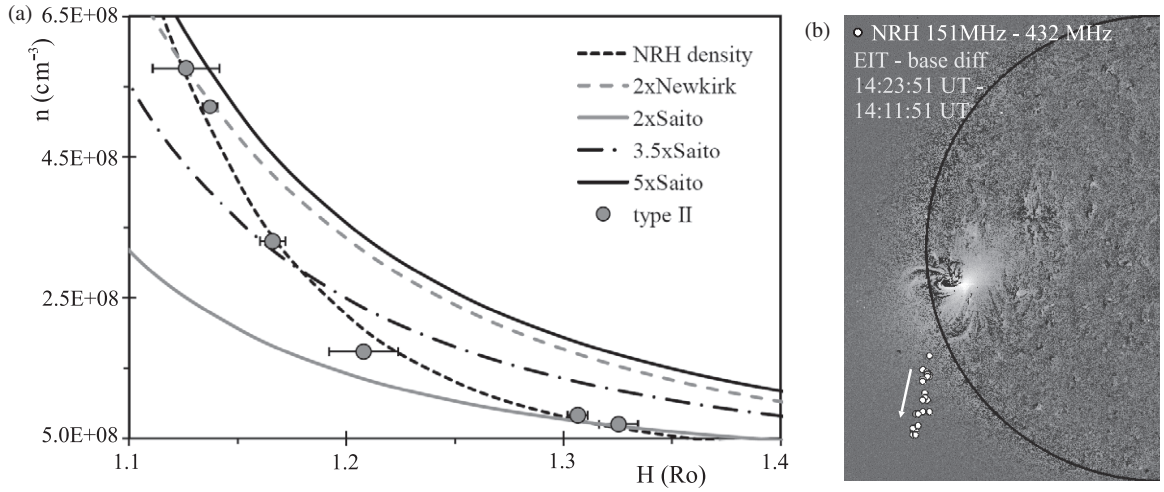

Figure 2. (a) Coronal electron density shown as a function of height (in solar radii $R_\odot$). The electron density profile obtained from the radio observations is presented with black circles and a black dashed line. For comparison, the radial dependence of the plasma density based on the models of Newkirk (1961) and Saito et al. (1970) is displayed. The observations show a decrease in the coronal electron density between fivefold Saito and twofold Saito density models. (b) NRH radio-source positions at 151, 164, 237, 327, 411, and 432 MHz corresponding to the low-frequency lane of the harmonic band of the type II burst overlaid on the base-difference *SOHO*/EIT 195 Å images (the last pre-event image is subtracted from the actual image). The white arrow indicates the direction of the NRH source propagation.

Table 1
Type II Speed (in km s^{-1}) Obtained by Applying Different Density Models

Density	Frequency Interval (MHz)		
Model	572–320	295–193	185–149
5× Saito	1370	1240	630
3.5× Saito	1130	1110	600
NRH	860	600	290
NRH, corrected[a]	990	700	330

Note. [a] Observations show that shock propagation was nonradial. The correction of the shock wave speed for the angle of 70° is introduced.

the type II burst were imaged in the whole frequency range covered by the NRH (Figure 1(b)). The estimated height of the NRH source (Figure 2(a)) at each observing frequency is an average value of a number of measurements. The scatter of the individual measurements is presented in Figure 2(a) by error bars. The NRH positions (the centroids of the radio sources) were better defined at the three highest observing frequencies. We used the positions of NRH sources corresponding to the lower frequency lane of the harmonic band of the type II burst, i.e., radio emission originating from the shock upstream region (hypothesis by Smerd et al. 1974, 1975) corresponding to the pre-shock corona. The positions of the NRH sources obtained were converted to heights above the photosphere H. For an estimation of the electron density n_e we employed the standard relationship $f \approx 9n_e^{1/2}$ (n_e is expressed in cm^{-3} and f in kHz).

Figure 2(a) shows a comparison of the NRH density profile obtained from the radio observations (gray circles and dashed black curve) and the radial dependence of the coronal plasma density in different models (Newkirk 1961; Saito et al. 1970). The NRH density profile was obtained by fitting the NRH data points. We used a gradient-expansion algorithm to compute the nonlinear least-squares fit to a function of an arbitrary number of parameters. The initial fitting functions were the Newkirk, Saito, and Mann density profiles (Newkirk 1961; Saito et al. 1970; Mann et al. 1999). The best fit was obtained with the Saito electron density profile as the initial fitting function. The observations show a decrease of the coronal electron density, i.e., the NRH density profile is placed between the 5× Saito (which is close to 2× Newkirk) and 2× Saito density models, with an average value of 3.5× Saito. The NRH density profile shows a rather steep density decrease in comparison to the other density models presented (Figure 2(a)). For the estimation of the type II speed, we used the largest and average density profiles, i.e., 5× and 3.5× Saito and the NRH density profile. The observations indicated a significant change in the type II speed, so the time interval during which the type II burst was observed was divided into three subintervals. We found that the type II speed decreased from 1370 to 1240 to 630 km s^{-1} when the density profile of 5× Saito was considered (Table 1). Using the average density profile of 3.5× Saito, we obtained speeds of 1130, 1110, and 600 km s^{-1} for the three intervals, respectively. The NRH density profile gave us somewhat smaller type II speeds of about 860, 600, and 290 km s^{-1} (see Table 1). Figure 2(b) shows the positions of NRH radio sources overlaid on the temporally closest base-difference EIT 195 Å image. The positions of the NRH sources (white circles) indicate that the propagation direction of the shock wave is not radial. The shock trajectory seems to be at an angle of about 70° with respect to the radial direction. This explains the somewhat smaller shock speeds obtained using the NRH density profile. If we take into account the nonradial propagation and consider the spherical distribution of the coronal electron density, we obtain corrected (for the factor of $1/\cos 70°$) speeds of about 990, 700, and 330 km s^{-1} (Table 1).

Additionally, for comparison with the type II speeds obtained by applying density models, we also estimated the type II burst speed directly using the positions of the corresponding NRH radio sources. Considering the NRH source positions at 432, 411, and 327 MHz, a plane-of-the-sky type II speed of about 1000 km s^{-1} was obtained. The type II speed obtained using the NRH positions at 327, 237, 164, and 151 MHz was about 550 km s^{-1} (see Table 2). The decrease in the type II speed indicates a rather strong deceleration of the radio source that is in agreement with the shock speed estimations mentioned above. The variation in the type II speeds listed in Tables 1 and 2 is probably due to the application of different density models and to the different frequency ranges in which the type II burst was

Table 2
Type II Speed (in km s^{-1}) Obtained by Measuring NRH Source Positions

NRH Source	Frequency Interval (MHz)	
Positions	432–327	327–151
NRH sources	1000	550
NRH sources, 30° correction[a]	1160	640
NRH sources, 45° correction[a]	1420	780

Note. [a] The correction of the shock wave speed for the possible projection effects on the plane of the sky is considered.

considered. These values also give an idea about uncertainties in the type II speed calculations. We also considered possible projection effects of the shock wave trajectory on the plane of the sky. Theoretically, the propagation angles with respect to the plane of the sky can be between 0° and 90°. In the case of large propagation angles (like 80° or 90°) with respect to the plane of the sky, the NRH sources would appear to be grouped more or less at the same position and propagation of the radio sources would not be visible. In the other extreme case, i.e., very small angles, the difference between true and observed type II speed would be very small.

Therefore, we considered the case of the type II radio source propagating at an angle of about 30° or 45°. When a projection of about 30° was considered, we obtained corrected type II speeds of 1160 and 640 km s^{-1} for the two frequency intervals mentioned earlier (Table 2). The projection of 45° gives corrected shock speeds of 1420 and 780 km s^{-1}. These two estimates of the shock wave speed agree well with the values deduced from the dynamic spectrum analysis using the 3.5× and 5× Saito density models (Tables 1 and 2).

2.3. Characteristics of the Associated Flare

The shock wave of 2005 November 14 was related to a *GOES* M3.9 flare (Figures 3(a) and (b)) from the NOAA AR 10822 (S06° E60°). The beginning, maximum, and end of this very impulsive flare were at 14:18:00, 14:21:40, and 16:30:00 UT, respectively. The SXR flare shows an exceptionally "spiky" profile with a fast rise, followed by a relatively fast decrease that eventually transformed into a prolonged decay. The SXI observations show the solar flare but no signatures of global coronal waves (Warmuth et al. 2005) or CMEs. Figure 4 shows the sequence of Hα images recorded by the KSO. The evolution of the Hα flare does not show a two-ribbon morphology, only a simple and confined flare brightening. The spatial resolution of Hα observations was too low to distinguish the possible fine structure of the source.

The high-energy solar flare emission associated with the impulsive phase of the *GOES* M3.9 flare was fully observed by *RHESSI*. The observations show that the X-ray sources of emission in the 6–12 keV band (dominated by thermal emission of plasma with temperatures $\gtrsim 10^7$ K) and 25–50 keV band (dominated by nonthermal emission of electron beams) are co-spatial (Figure 5). This implies that the emission originates mainly from a small region, i.e., the same source in the corona, and/or from a very small and unresolved loop (less than 5 arcsec). We conclude that the majority of the *RHESSI* soft and hard X-ray emission is from the solar corona. Only a small extension toward the footpoints is seen in the 25–50 keV images (Figure 5). Even with the finest grid, it was possible to identify only one footpoint source. The light curves of the nonthermal bands, 25–50 and 50–100 keV, show two peaks

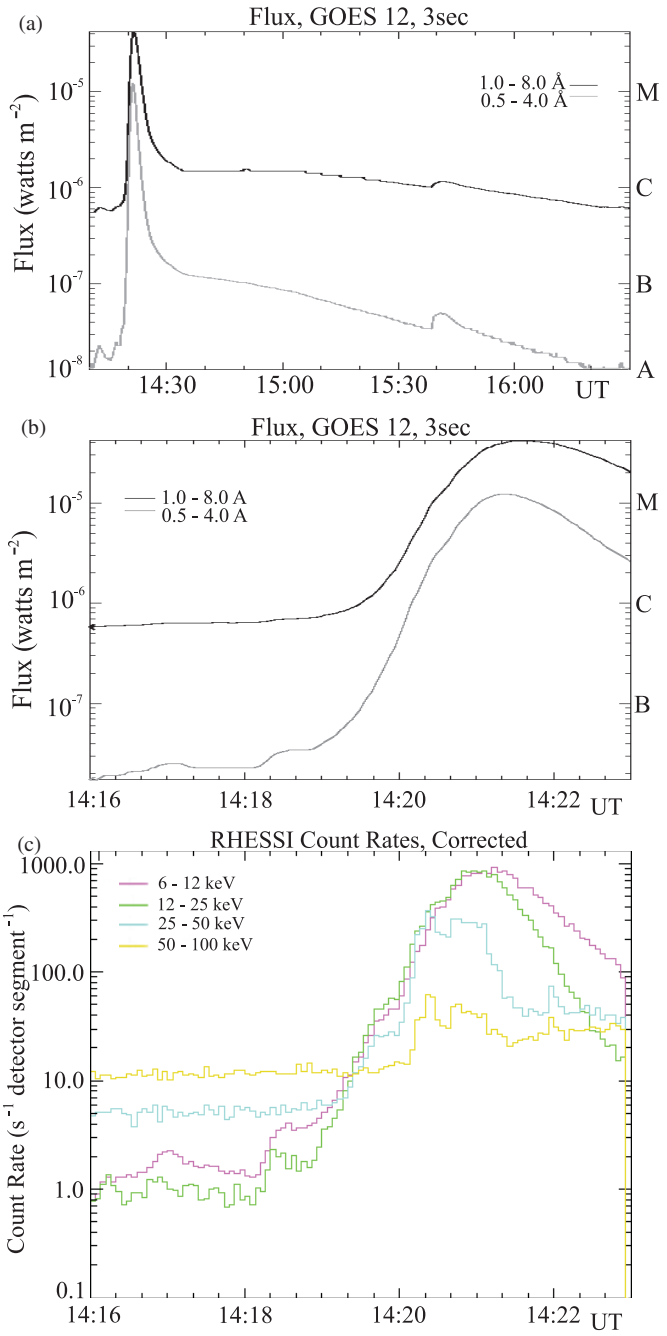

Figure 3. (a) The *GOES* M3.9 flare profile shows a very impulsive energy release. (b) Zoom to the rising phase of the SXR flare observed by *GOES*. (c) *RHESSI* corrected count rates in four energy intervals from 6 to 100 keV. Two peaks of the nonthermal bands (25–50 and 50–100 keV) are rather well correlated with the microwave radio emission observed with Phoenix 2.
(A color version of this figure is available in the online journal.)

(each of duration of about 20–30 s) at about 14:20:20 and 14:20:44 UT (Figure 3(c)).

From the *RHESSI* images in the 6–12 keV band we inferred a volume $V \sim A^{1.5} \approx 2 \times 10^{26}$ cm^3 (where A is the emitting area). This dependence follows from the dimensionality, since $V \sim R^3$ and $A \sim R^2$.

Additionally, from the emission measure EM $\approx 0.15 \times 10^{49}$ cm^{-3} and the volume V, we inferred a density $n \approx (\mathrm{EM}/V)^{0.5} \approx 10^{11}$ cm^{-3}. The density obtained is unusually high, and the temperature is about 24 MK. All this suggests

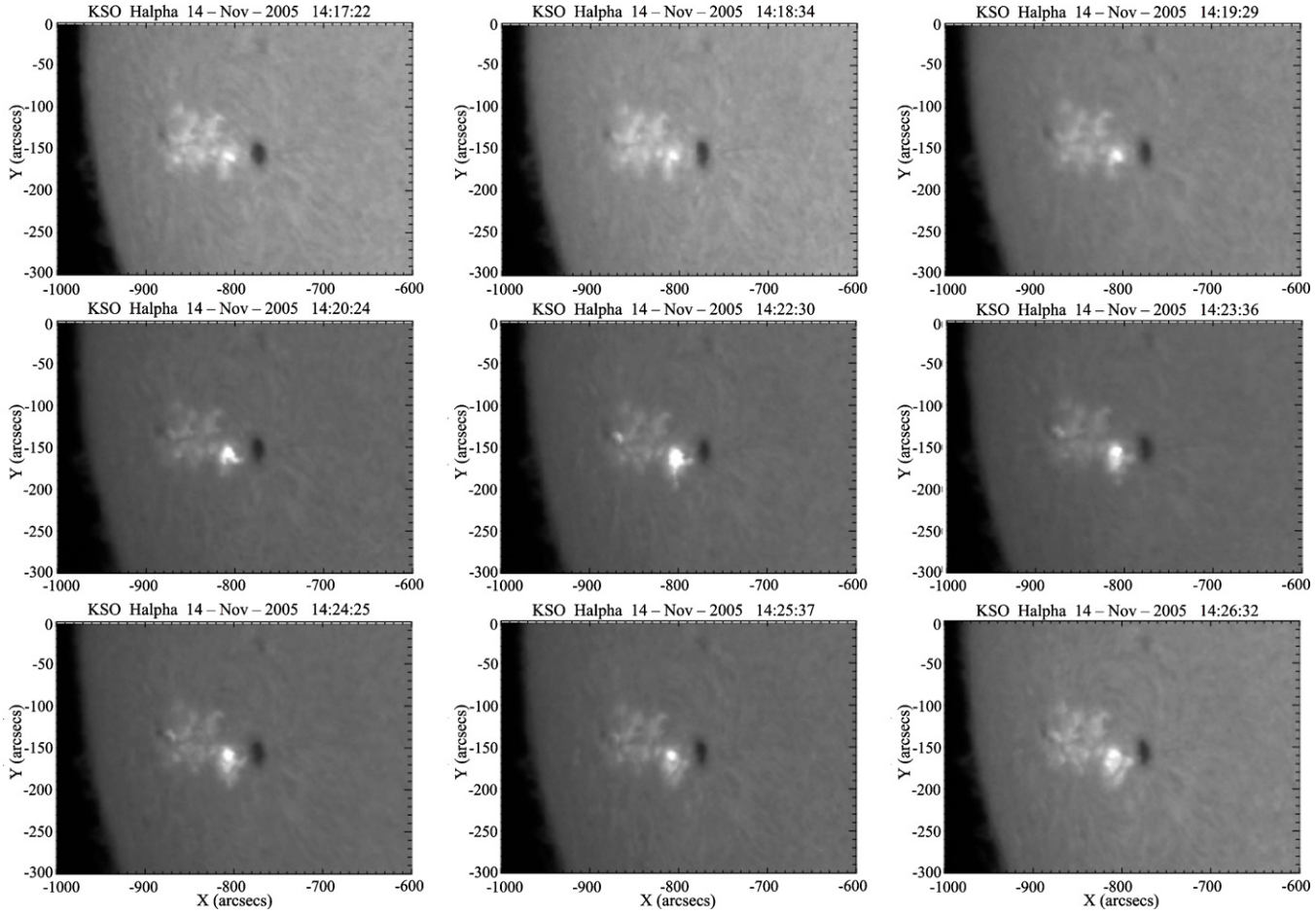

Figure 4. Hα images of the 2005 November 14 flare, recorded by the Kanzelhöhe Observatory. Hα observations show a simple brightening of a confined and a very compact flare.

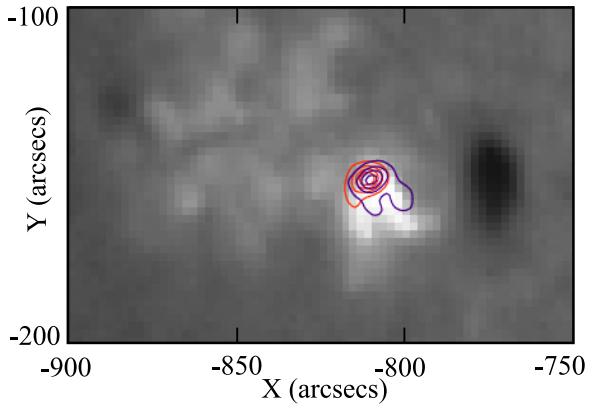

Figure 5. Hα image of the 2005 November 14 flare with superposed *RHESSI* contours in the 6–12 keV and 25–50 keV bands (red and blue contours, respectively).

(A color version of this figure is available in the online journal.)

a very strong, impulsive increase in pressure in the small flare loop during the peaks of X-ray emission (duration 20–30 s).

2.4. EUV and Coronagraph Observations

The EIT observations at 195 Å show a brightening of pre-flare loops, the first signatures of the flare at 14:23:51 UT, and oscillations of loops in the vicinity of the flare site. However, signatures of rising loops or any other rising structure as possible early signatures of the CME were not observed in the EUV. Further on, the EUV observations also do not show an associated EIT wave as a possible surface signature of the CME (Thompson et al. 2000; Chen et al. 2005).

On the other hand, the 195 Å base-difference EIT images show rather weak and moderate size dimming, first observed at 14:35:51 UT (Figure 6(a)). The coronal dimming corresponds to the change in the physical conditions of the emitting plasma and is usually considered to be an early CME signature (e.g., Hudson & Cliver 2001). However, in this particular event dimming might not have been caused by the mass evacuation. Namely, although the flare appeared close to the solar limb and the geometry was favorable for the detection of an associated CME, LASCO observations (in LASCO C2 and LASCO C3 fields of view) do not show any signatures of a CME associated with the shock wave observed at 14:21:40 UT. The LASCO CME catalog (Yashiro et al. 2004) does not report any CME associated with the flare on 2005 November 14 either. The CME temporally closest to the type II radio burst was first observed in the LASCO C2 field of view at 08:30:05 UT, almost 6 hr before the shock wave signatures, at a height of 2.69 $R_{\odot}$. The CME was very slow, propagating at a speed of about 180 km s^{-1}. Figure 6(b) shows LASCO C2 running difference images in the time interval 14:30–15:30 UT. We observed only very weak signatures of a diffuse, almost stationary, remnant of the east-side leg (marked with white arrows) of this partial halo CME. Figure 6(c) (LASCO C3 running difference images) shows the leading edge of the CME at 14:18:05 UT at a height of 7.06 $R_{\odot}$.

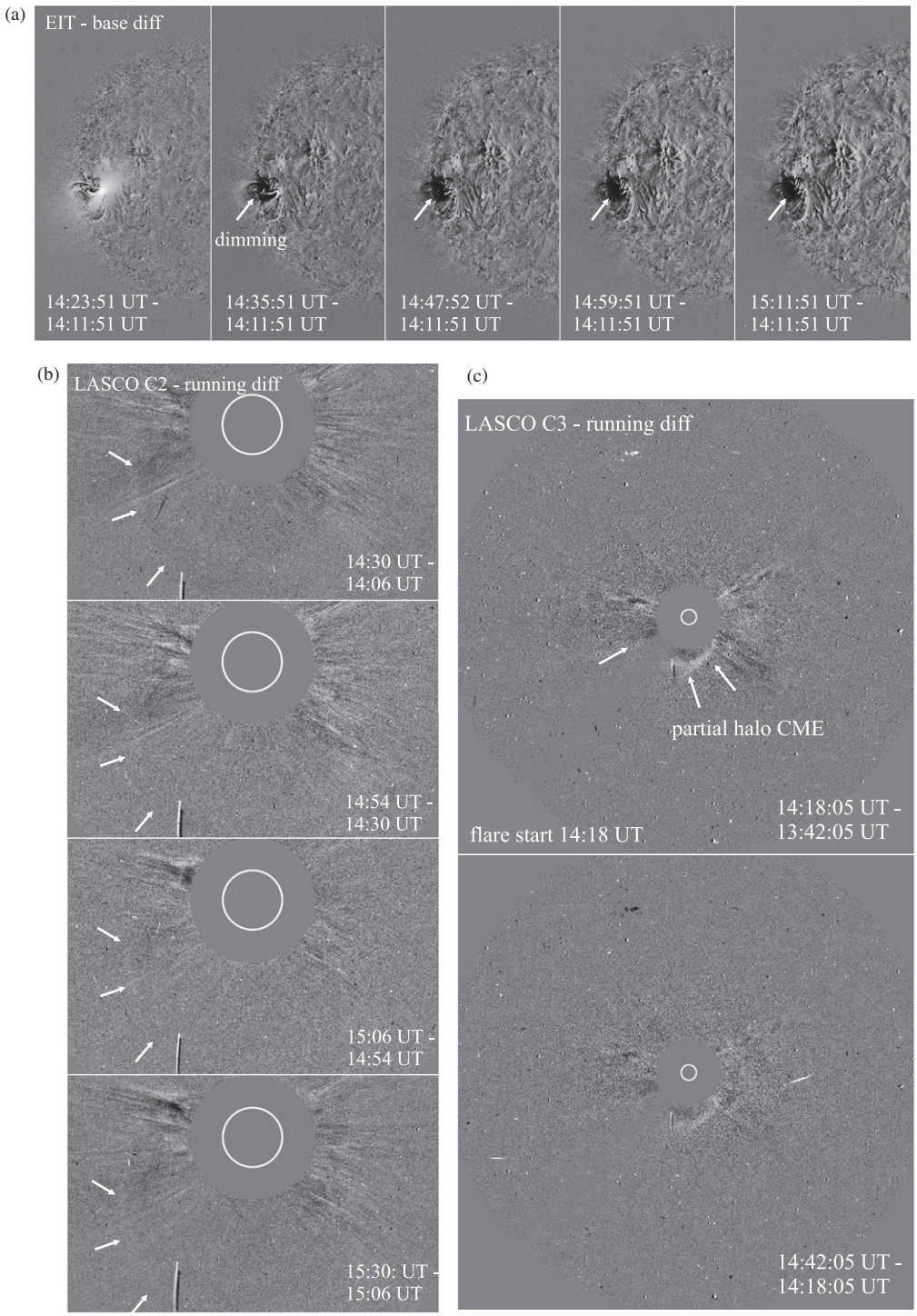

Figure 6. (a) Base-difference EIT images (the pre-event image is subtracted from other images) show the flare and rather small size dimming. (b) LASCO C2 running difference images (the previous image of a sequence is subtracted from every image) show very weak signatures of a remnant of a partial halo CME (marked by white arrows). (c) LASCO C3 running difference images show the CME signatures at 14:18:05 UT at a height of 7.06 $R_{\odot}$. This CME was not associated with the shock wave on 2005 November 14 (see the text).

We note that the type II radio burst appeared at 14:21:40 UT at a height of 1.14 $R_{\odot}$. Clearly, observations show that this CME can be excluded as a potential driver of the observed coronal shock wave.

Coronal dimmings are often considered to be reliable signature of CMEs (see, e.g., Hudson & Cliver 2001; Zhukov & Auchère 2004). In this event, if the dimming reflects the presence of a CME, that CME should be very weak because it was not observed by LASCO, although the source region was close to the limb. Weak and diffuse CMEs are usually not energetic, and it is unlikely that such a CME would attain a speed higher than the local Alfvén speed (700 km s^{-1}) to drive a shock wave.

3. SUMMARY AND CONCLUSIONS

In this paper, we presented a multi-wavelength study of a shock wave manifested by a high-frequency type II radio burst that occurred on 2005 November 14. The particularity of the

event is that the coronagraph observations do not show any clear signatures of an associated CME although the flare occurred close to the solar limb and the geometry was favorable for the detection of a possibly associated CME.

The close-to-limb position of the flare implies that the projection effects in estimating the shock wave speed are small. The type II source was observed at all six NRH frequencies, which enabled us to estimate the trajectory of the radio source. Due to such good coverage by NRH observations, it was also possible to estimate the shock wave speed using two different methods (Tables 1 and 2). Comparison of radio and EUV observations enabled us to make corrections for projection effects in the speed estimation. We found that the shock wave propagated with an initial speed of 1300–900 km s^{-1} and decelerated to a speed of about 600–300 km s^{-1}. The velocity decrease of the shock wave is consistent with a flare-generated blast wave (e.g., Vršnak & Cliver 2008).

The shock was associated with a very impulsive *GOES* M3.9 flare (rise time <4 minutes), similar to the recently reported CME/flare events where the shock waves were generated by impulsive flares (Magdalenić et al. 2008, 2010). Since we did not observe any associated ejecta and/or CMEs, we classified this flare as a confined flare (see, e.g., Svestka 1986; Cliver 1995) or a CME-less flare (Klein et al. 2010). Hα observations showed that this impulsive flare was also very compact. This was confirmed by *RHESSI* observations, which show a compact event of a rather high density ($n \approx 10^{11}$ cm^{-3}) and high temperature (24 MK). *RHESSI* observations suggest the scenario of a strong, impulsive increase in pressure in the small flare volume. All this indicates that a shock wave was ignited by the flare.

While SXI observations show the solar flare and no signatures of a mass ejection, EIT observations show a weak dimming, suggesting the possible presence of a CME. However, although the flare originated from an active region close to the limb and the geometry was favorable for detection of an associated CME, LASCO C2 and C3 observations do not show any CME possibly associated with the event. Since we do not observe any associated ejecta or other signatures of an associated CME in the coronagraph observations, we conclude that the dimming was not caused by the expansion and opening of magnetic field lines during the early phase of a CME. Even if we consider that the observed dimming reflects the presence of a CME, it does not seem probable that such a weak CME (not observed by a coronagraph) could drive the fast shock wave on 2005 November 14.

It was recently shown that a specific class of CME/flare events associated with flare-generated shock waves exists (Magdalenić et al. 2008, 2010). However, these works do not exclude the possibility that the presence of a mass ejection, i.e., a CME, might be a necessary condition for shock formation (see, e.g., Vršnak et al. 2006). Additionally, numerous studies performed in the last few decades showed that CMEs play a very important role in the formation of coronal shock waves (e.g., Thompson et al. 2000; Gopalswamy et al. 2005; Vršnak & Cliver 2008). The present study demonstrates that, although probably in rather rare cases, the coronal shock wave can be generated by a flare without the presence of an associated CME. We conclude that the presence of a CME is not a necessary condition for coronal shock formation.

The EIT and LASCO data used in this study are courtesy of the *SOHO*/EIT and *SOHO*/LASCO consortiums, respectively. The CME catalog is generated and maintained at the CDAW Data Center by NASA and The Catholic University of America in cooperation with the Naval Research Laboratory. *SOHO* is a project of international cooperation between ESA and NASA. We are grateful to the staff of the Nançay Radioheliograph (Paris Observatory), the Green Bank Solar Radio Burst Spectrometer (National Radio Astronomy Observatory), and the Astrophysical Institute Potsdam for their open data policy. The research leading to these results received funding from the European Commission's Seventh Framework Programme (FP7/2007-2013) under grant 218816 (SOTERIA project, www.soteria-space.eu). We are grateful to N. Gopalswamy and A. Vourlidas for helpful discussions.

REFERENCES

Bougeret, J.-L., Kaiser, M. L., Kellogg, P. J., et al. 1995, Space Sci. Rev., 71, 231
Brueckner, G. E., Howard, R. A., Koomen, M. J., et al. 1995, Sol. Phys., 162, 357
Chen, P. F., Fang, C., & Shibata, K. 2005, ApJ, 622, 1202
Cho, K., Lee, J., Gary, D. E., Moon, Y., & Park, Y. D. 2007, ApJ, 665, 799
Cliver, E. W. 1995, Sol. Phys., 157, 285
Cliver, E. W., Nitta, N. V., Thompson, B. J., & Zhang, J. 2004, Sol. Phys., 225, 105
Delaboudinière, J.-P., Artzner, G. E., Brunaud, J., et al. 1995, Sol. Phys., 162, 291
Gopalswamy, N., Aguilar-Rodriguez, E., Yashiro, S., et al. 2005, J. Geophys. Res. (Space Phys.), 110, 12
Gopalswamy, N., Kaiser, M. L., Lepping, R. P., et al. 1998, J. Geophys. Res., 103, 307
Hill, S. M., Pizzo, V. J., Balch, C. C., et al. 2005, Sol. Phys., 226, 255
Hudson, H. S., & Cliver, E. W. 2001, J. Geophys. Res., 106, 25199
Karlicky, M. 1984, Sol. Phys., 92, 329
Kerdraon, A., & Delouis, J.-M. 1997, in Proc. CESRA Workshop on Coronal Physics from Radio and Space Observations, ed. G. Trottet (Lecture Notes in Physics, Vol. 483; Berlin: Springer), 192
Khan, J. I., & Aurass, H. 2002, A&A, 383, 1018
Klassen, A., Aurass, H., Klein, K., Hofmann, A., & Mann, G. 1999, A&A, 343, 287
Klassen, A., Pohjolainen, S., & Klein, K. 2003, Sol. Phys., 218, 197
Klein, K., Trottet, G., & Klassen, A. 2010, Sol. Phys., 263, 185
Lecacheux, A. 2000, in Radio Astronomy at Long Wavelengths, ed. R. G. Stone, K. W. Weiler, M. L. Goldstein, & J.-L. Bougeret (Washington, DC: AGU), 321
Lin, R. P., Dennis, B. R., Hurford, G. J., et al. 2002, Sol. Phys., 210, 3
Liu, Y., Luhmann, J. G., Bale, S. D., & Lin, R. P. 2009, ApJ, 691, L151
Ma, S., Raymond, J. C., Golub, L., et al. 2011, ApJ, 738, 160
Magdalenić, J., Marqué, C., Zhukov, A. N., Vršnak, B., & Žic, T. 2010, ApJ, 718, 266
Magdalenić, J., Vršnak, B., Pohjolainen, S., et al. 2008, Sol. Phys., 253, 305
Mancuso, S., Raymond, J. C., Kohl, J., et al. 2002, A&A, 383, 267
Mann, G., Aurass, H., Voigt, W., & Paschke, J. 1992, in Coronal Streamers, Coronal Loops, and Coronal and Solar Wind Composition, ed. C. Mattok (ESA Special Publication, Vol. 348; Noordwijk: ESA), 129
Mann, G., Jansen, F., MacDowall, R. J., Kaiser, M. L., & Stone, R. G. 1999, A&A, 348, 614
Mann, G., & Klassen, A. 2005, A&A, 441, 319
Maričić, D., Vršnak, B., Stanger, A. L., et al. 2007, Sol. Phys., 241, 99
Messmer, P., Benz, A. O., & Monstein, C. 1999, Sol. Phys., 187, 335
Moreton, G. E., & Ramsey, H. E. 1960, PASP, 72, 357
Nelson, G. J., & Melrose, D. B. 1985, in Solar Radiophysics: Studies of Emission from the Sun at Metre Wavelengths, ed. D. J. McLean & N. R. Labrum (Cambridge: Cambridge Univ. Press), 333
Newkirk, G. J. 1961, ApJ, 133, 983
Nindos, A., Alissandrakis, C. E., Hillaris, A., & Preka-Papadema, P. 2011, A&A, 531, A31
Nindos, A., Aurass, H., Klein, K.-L., & Trottet, G. 2008, Sol. Phys., 253, 3
Ontiveros, V., & Vourlidas, A. 2009, ApJ, 693, 267
Otruba, W., & Pötzi, W. 2003, Hvar Obs. Bull., 27, 189
Pizzo, V. J., Hill, S. M., Balch, C. C., et al. 2005, Sol. Phys., 226, 283
Pohjolainen, S. 2008, A&A, 483, 297
Pohjolainen, S., Pomoell, J., & Vainio, R. 2008, A&A, 490, 357
Roberts, J. A. 1959, Aust. J. Phys., 12, 327

Saito, K., Makita, M., Nishi, K., & Hata, S. 1970, Ann. Tokyo Astron. Obs., 12, 51
Smerd, S. F., Sheridan, K. V., & Stewart, R. T. 1974, in IAU Symp. 57, Coronal Disturbances, ed. G. A. Newkirk (Cambridge: Cambridge Univ. Press), 389
Smerd, S. F., Sheridan, K. V., & Stewart, R. T. 1975, Astrophys. Lett., 16, 23
Svestka, Z. 1986, in Proc. Solar Maximum Mission Symposium, The Lower Atmosphere of Solar Flares, Sunspot, NM, 1985 August 20–24, ed. D. F. Neidig (A87-26201 10-92; Sunspot, NM: National Solar Observatory), 332
Temmer, M., Veronig, A. M., Kontar, E. P., Krucker, S., & Vršnak, B. 2010, ApJ, 712, 1410
Temmer, M., Veronig, A. M., Vršnak, B., et al. 2008, ApJ, 673, L95
Thompson, B. J., Reynolds, B., Aurass, H., et al. 2000, Sol. Phys., 193, 161
Vourlidas, A., Wu, S. T., Wang, A. H., Subramanian, P., & Howard, R. A. 2003, ApJ, 598, 1392
Vršnak, B., Aurass, H., Magdalenić, J., & Gopalswamy, N. 2001, A&A, 377, 321
Vršnak, B., & Cliver, E. W. 2008, Sol. Phys., 253, 215
Vršnak, B., Magdalenić, J., Aurass, H., & Mann, G. 2002a, A&A, 396, 673
Vršnak, B., Magdalenić, J., & Zlobec, P. 2004, A&A, 413, 753
Vršnak, B., Warmuth, A., Brajša, R., & Hanslmeier, A. 2002b, A&A, 394, 299
Vršnak, B., Warmuth, A., Temmer, M., et al. 2006, A&A, 448, 739
Warmuth, A. 2007, in The High Energy Solar Corona: Waves, Eruptions, Particles, ed. K.-L. Klein & A. L. MacKinnon (Lecture Notes in Physics, Vol. 725; Berlin: Springer), 107
Warmuth, A., Mann, G., & Aurass, H. 2005, ApJ, 626, L121
Warmuth, A., Vršnak, B., Magdalenić, J., Hanslmeier, A., & Otruba, W. 2004, A&A, 418, 1101
White, S. M., Bastian, T. S., & Bradley, R. 2007, in NRAO Newsletter, ed. M. T. Adams (Charlottesville, VA: NRAO), Vol. 110, 9
White, S. M., Bastian, T. S., Bradley, R., Parashare, C., & Wye, L. 2005, in ASP Conf. Ser. 345, From Clark Lake to the Long Wavelength Array: Bill Erickson's Radio Science, ed. N. Kassim, M. Perez, W. Junor, & P. Henning (San Francisco, CA: ASP), 176
Wild, J. P. 1950, Aust. J. Sci. Res. A Phys. Sci., 3, 399
Yashiro, S., Gopalswamy, N., Michalek, G., et al. 2004, J. Geophys. Res. (Space Phys.), 109, 7105
Zhang, J., Dere, K. P., Howard, R. A., Kundu, M. R., & White, S. M. 2001, ApJ, 559, 452
Zhukov, A. N., & Auchère, F. 2004, A&A, 427, 705